Journal of Hydrology 572 (2019) 40–50

Contents lists available at ScienceDirect

Journal of Hydrology

journal homepage: www.elsevier.com/locate/jhydrol

Research papers

Seasonal and interannual variations of hydrochemical characteristics and stable isotopic compositions of drip waters in Furong Cave, southwest China based on 12 years' monitoring

Jian Zhang[a,b], Ting-Yong Li[a,b,*,1]

[a] Chongqing Key Laboratory of Karst Environment, School of Geographical Sciences, Southwest University, Chongqing 400715, China
[b] Field Scientific Observation & Research Base of Karst Eco-environments at Nanchuan in Chongqing, Ministry of Nature Resources of China, Chongqing 408435, China

ARTICLE INFO

This manuscript was handled by Peter K. Kitanidis, Editor-in-Chief, with the assistance of Dongmei Han, Associate Editor

Keywords:
Drip water
Trace element ratios
Stable isotopes
PCP/ICD/WRI
Rainfall

ABSTRACT

Cave monitoring is crucial for the interpretation of climatic and environmental significances of various geological proxies in speleothem. Therefore, the hydrochemical and stable isotopic compositions ($\delta^{18}O$, δD, Mg/Ca, Sr/Ca, and Ba/Ca) of karst cave waters during 2005–2016 CE were constantly monitored in Furong Cave, Chongqing City, Southwest China. A comparison with local hydrological conditions led to 4 main conclusions as follows: (1) the Mg/Ca ratio is significantly responsive to the changes in drought/wet conditions outside the cave, which increased in drought years and decreased in wet years, respectively. Seasonal variation of Sr/Ca is more significant than those of Mg/Ca and Ba/Ca ratios. (2) Prior calcite precipitation (PCP), incongruent calcite dissolution (ICD), water–rock interaction (WRI), and pCO_2 of soil and cave air, may account for the changes in trace element ratios in the epikarst, which resulted in a complex variation of element ratios in the cave drip water. In general, WRI in drought years is stronger than that in wet years, and that in low discharge sites is stronger than in high discharge sites. Seasonal variation of Ca^{2+} concentration, induced by PCP, exerts significant impact on the evolution of Sr/Ca ratio in drip water. (3) $\delta^{18}O$ and δD of drip water are influenced by the "mixing effect", leading to the result that their seasonal variations are less significant than that of precipitation. (4) At least in the study period, the ratios of trace elements in the drip water in Furong Cave mainly reflected the variations of local hydrological conditions (drought or wet) dominated by precipitation. Because of the "mixing effect" of groundwater, high-resolution $\delta^{18}O$ record (e.g., seasonal and annual) of speleothem in Furong Cave may not be recommendable. However, the $\delta^{18}O$ is potentially a reliable proxy in speleothems to record the change of rainfall on decadal and longer timescales.

1. Introduction

As geological carriers for paleoclimate change, speleothems are mostly composed of calcium carbonate, with multiple-proxies such as $\delta^{18}O$, $\delta^{13}C$, and trace element ratios. These proxies were used for the reconstruction of paleorainfall, paleovegetation, paleohydrogeology, and paleoenvironment (Roberts et al., 1998; Lauritzen and Lundberg, 1999; Wang et al., 2001, 2008; Yuan et al., 2004; Johnson et al., 2006; Fairchild and Treble, 2009; Cheng et al., 2009, 2012, 2016; Jo et al., 2010; Wong and Breecker, 2015). Owing to the fact that controlling factors of the proxies of speleothem are numerous and complex, interpretation of climate information based on these proxies is controversial (McDermott et al., 1999; Fairchild et al., 2006). However, cave drip water, a signal transmitter between speleothems and external climate environment, is of great significance to explore the depositional mechanism of speleothem and interpret the climate information from various proxies (Tooth and Fairchild, 2003; Oster et al., 2012).

The negative isotope excursion with the increased precipitations, namely "amount effect", have been widely accepted in the communities of paleoclimate (Dansgaard, 1964). However, many studies also have suggested that a direct link between the speleothem $\delta^{18}O$ records and precipitation is debatable. Liu et al. (2015) found that the strongest period of the East Asian Summer monsoon (EASM) occurred in the early Holocene period referred from the Chinese speleothem $\delta^{18}O$ record, challenging the view of mid-Holocene EASM maximum based on lakes, loess, and pollen records from northern China, and all of these Holocene Chinese speleothem $\delta^{18}O$ records also exhibited a similar trend of variation indicating a common climate signal (e.g., rainfall or Asian

* Corresponding author at: No. 2 Tiansheng Road, Beibei District, Chongqing 400715, China.
E-mail address: cdlty@swu.edu.cn (T.-Y. Li).
[1] Joint first author.

https://doi.org/10.1016/j.jhydrol.2019.02.052
Received 8 September 2018; Received in revised form 20 February 2019; Accepted 28 February 2019
Available online 28 February 2019
0022-1694/ © 2019 Elsevier B.V. All rights reserved.

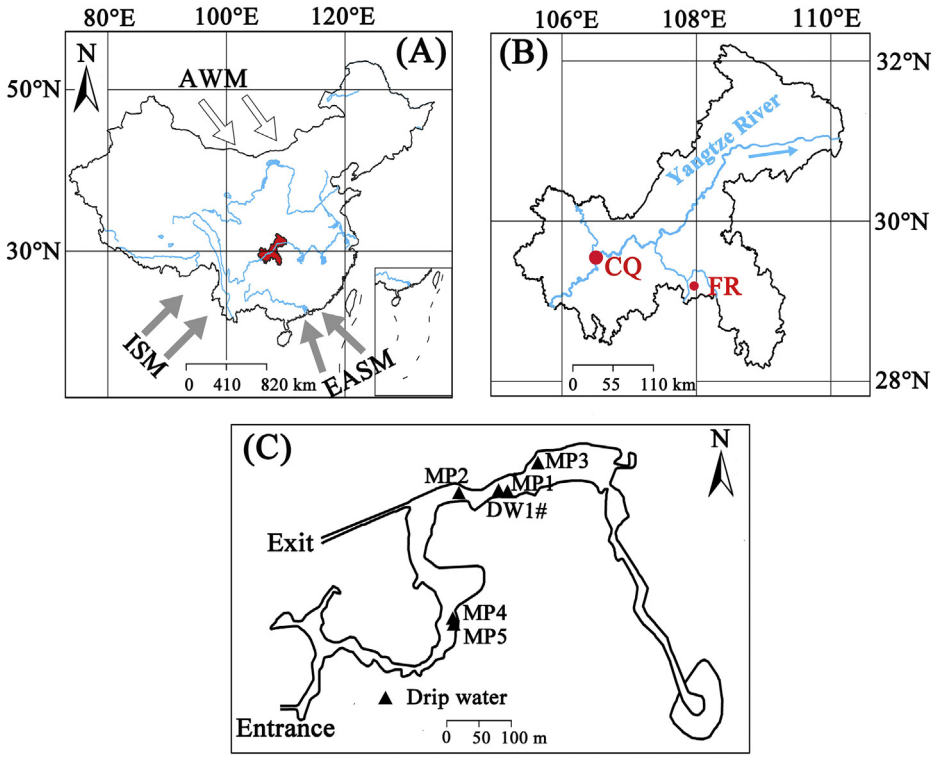

Fig. 1. (A) Location of the study area, Furong Cave in Southwest China. Gray arrows indicate Indian Summer monsoon (ISM) and East Asian Summer monsoon (EASM). White arrows indicate Asia Winter monsoon (AWM). The red area indicates the location of Chongqing City. (B) Locations of Furong Cave (FR) and the urban areas of Chongqing City (CQ) (red solid dots). The Yangtze River flows across Chongqing municipality city from the southwest to the northeast. (C) Distribution of monitoring sites (black triangles) in Furong Cave (DW1# and MP1–MP5; all of them are drip water sites) (Modified after Li et al., 2011). (For interpretation of the references to colour in this figure legend, the reader is referred to the web version of this article.)

summer monsoon intensity). However, the instrumental data and models indicated a significant different spatial variation in rainfall between northern and southern China (Liu et al., 2015). Therefore, it is believed that the speleothem $\delta^{18}O$ cannot represent the changes in intensity of EASM accurately (Liu et al., 2015, 2017). On the other hand, inconsistency between speleothem $\delta^{18}O$ records and solar radiation in northern hemisphere have been noted, and Clemens et al. suggested that the speleothem $\delta^{18}O$ in the Asian monsoon region may not be a simple proxy for the intensity of summer monsoon, which may also reflect the changes in moisture sources and transport pathway (Clemens et al., 2010). Some studies have presented that on interannual to decadal timescales, the $\delta^{18}O$ and δD values of precipitation were significantly affected by the changes in moisture sources, which could be attributed to the changes in atmospheric circulation, such as El Niño-Southern Oscillation (ENSO) (Tan, 2014, 2016), recorded changes in Asian summer monsoon (ASM) intensity, and the effect of rainfall in the upper reaches on moisture source (Yang et al., 2016).

The trace elements in cave water mainly come from bedrock and soil (Zhou et al., 2009, 2012). A series of physical and chemical processes in epikarst, including water–rock interaction (WRI), prior calcite precipitation (PCP), incongruent calcite dissolution (ICD), mixing of old and fresh water, and dilution effects by fracture water in the bedrock, may affect the changes in trace element ratios in cave drip water and speleothem (Tooth and Fairchild, 2003; Spötl et al., 2005; Sherwin and Baldini, 2011). The above-mentioned factors which may affect the changes of trace element ratios in drip water have direct or indirect links with precipitation. The combination of $\delta^{18}O$ and trace element ratios is important for the reconstruction of paleoclimate based on speleothems (Oster et al., 2012). However, there is a lack of testing with long-time monitoring data for whether or not the $\delta^{18}O$ or trace element ratios can reflect the changes in precipitation.

In this paper, we summarized the 12-year monitoring work in Furong Cave, southwest China, and presented a comprehensive analysis on the interannual and seasonal variation of trace element ratios, $\delta^{18}O$ and δD of drip water. Combined with the changes in atmospheric circulation characterized by ENSO, and the changes in local temperature and precipitation, we discussed the response of $\delta^{18}O$, δD, and trace element ratios of drip water to external climate signals. This paper is mainly focused on the following scientific questions: (1) Are there any difference between the responses of element ratios and isotopic compositions of cave drip water corresponding to the external environment? (2) Whether or not the change of elements ratios made response to extreme flood and drought events outside Furong Cave, which is covered by 300–500 m thick bedrock? (3) Whether or not drip water $\delta^{18}O$ values preserve high-resolution (e.g., seasonal, annual) signals from meteoric precipitation?

Note that the 300 to 500 m aquifer zone above Furong Cave is far thicker than other monitoring caves in EASM region, such as Xianren Cave (40–140 m), Liangfeng Cave (80–140 m), Shihua Cave (30–130 m) and so on (Luo and Wang, 2008; Cai et al., 2010; Duan et al., 2012), exhibiting some differences in hydrochemical characteristics and stable isotopic compositions of drip waters in Furong Cave. One of the most important reasons is the different residence time of ground water for each cave, because of the different thickness of overlying bedrock. Data interpretations for short monitoring durations are complicated by mostly unknown water transit times through the karst. Our exceptionally long monitoring work allows comparing confidently with hydrological factors related to rainfall changes and variations in the epikarst.

In addition, previous studies commonly analyzed single indicator in drip water (e.g., $\delta^{18}O$, element ratios or $\delta^{13}C$) (Li et al., 2011, 2012; Duan et al., 2016; Li and Li, 2018), but comprehensive studies combining $\delta^{18}O$ and trace element ratios are rarely reported. The main objective of this study is to distinguish the climate implications of the multiple-proxies (e.g., $\delta^{18}O$ and trace element ratios) in cave drip water. We do believe that the inferences of this long monitoring study are significant for the interpretation of climatic implications of the proxies in speleothems.

2. Study area

2.1. Physical geography background

Chongqing is located in the southwest region of China. The local

climate is characterized by the subtropical humid monsoon climate, which is dominated by East Asian Summer monsoon (EASM) and Indian Summer monsoon (ISM) in the summer months and by Asian Winter monsoon (AWM) in the winter months (Fig. 1A). Furong Cave (29°14′N, 107°55′E) is located in Wulong County, Chongqing City, on the east bank of Furongjiang River, a branch of Yangtze River. Furong Cave developed in the Middle Cambrian dolomite limestone strata and the local topography is characterized by a typical steep karst gorge (Li et al., 2011). The altitude at the entrance of Furong Cave is approximately 480 m above the sea level (a.s.l) (Appendix Fig. 1B), and the main tunnel is approximately 2800 m in length, 30–50 m in height, and 2–30 m in width. Furong Cave belongs to Tianxing-Furong cave karst system, which is a typical karst area of carbonate aquifer characterized by high permeability to absorb, store and transmit precipitation (Zhu et al., 2007). Another hydrogeological feature is that the 300–500 m thick aquifer zone above Furong Cave leads to numerous complex flow paths of groundwater (Li et al., 2011).

The relative humidity of cave air is close to 95–100%, and the average temperature is 16–16.3 °C in the inner chamber of Furong Cave (Li et al., 2011). In the 12-year monitoring period from 2005 to 2016, the average annual rainfall was 1079 mm outside Furong Cave. In general, in the rainy season from April to October every year, the precipitation accounted for over 85% of the total precipitation, and the annual average temperature was ~17.9 °C outside Furong Cave (Fig. 2H).

2.2. Monitoring sites

Five soil CO_2 monitoring sites, namely SA, SB, SC, SD, and SE, were set up along both sides of the valley overlying Furong Cave (Appendix Fig. 1A) (Li et al., 2012; Li and Li, 2018). The pipelines for soil CO_2 monitoring were buried in the soil profiles at the depth of 50 cm. Six drip water monitoring sites (DW1#, MP1, MP2, MP3, MP4, and MP5) were set up in Furong Cave (Fig. 1C; Li et al., 2011). DW1# and MP1 were 3 m apart with the drip height being approximately 22 m, split into multi-drip during the process of falling. Drip site MP2 was located on the top of a speleothem, 2 m in height, with the falling height being 27 m. MP3 was on the cavity wall, with a short soda-straw stalactite as the outlet, and the drip height was approximately 30 cm (Li et al., 2011). MP4 and MP5 were approximately 1.5 m apart with each other, and the drip heights were 14 m and 13 m, respectively (Li et al., 2012). The deposition rates of active sediments were 0.87, 5.69, 0.71, 5.31, and 4.13 mg/day, respectively, at the five drip water monitoring sites (MP1, MP2, MP3, MP4, and MP5) (Huang et al., 2015).

3. Data and methods

3.1. Meteorological data

During the period of year 2005–2016, a portable meteorological station was set up outside Furong Cave to collect meteorological data. Precipitation was recorded using an automatic rainfall monitoring instrument (RG3-M, Onset, USA) at a frequency of once every 2 min, with the precision being ± 1.0%. The air temperature was continuously recorded at 2-h intervals by the U12-011 temperature recorder (Onset, USA), with an error of ± 0.1 °C. The monthly average rainfall and air temperature outside Furong Cave were calculated on the basis of the recorded meteoric data, which were downloaded via the HOBO software every month.

The drought years and the wet years were distinguished according to the precipitation anomaly percentage, which was calculated as follows:

$$Dp = (P - \bar{P})/ P \times 100\% \quad (1)$$

where Dp is the percentage of precipitation anomaly, P is the annual precipitation in the year, and $\bar{P}$ is the average multi-year precipitation.

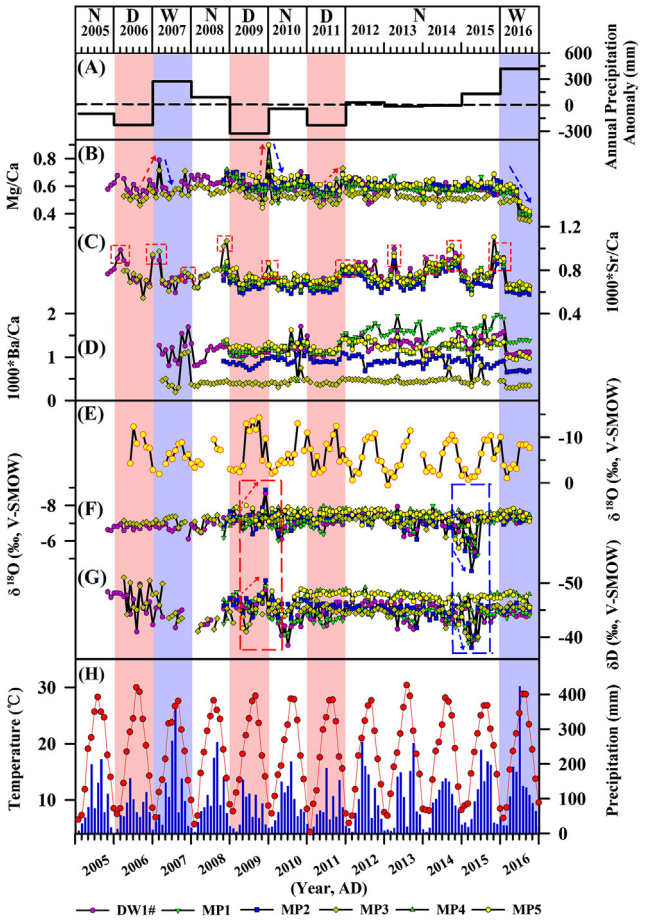

Fig. 2. The combined time series of meteoric conditions and the hydrogeochemistry of drip water. (A) Annual precipitation anomaly (mm), the horizontal dashed line means the average value for the annual rainfall during the monitoring period from 2005 to 2016. The letters "D" and "W" indicate the drought and wet years, respectively. (B) Diagrams showing the ratios of Mg/Ca, (C) 1000*Sr/Ca, and (D) 1000*Ba/Ca of drip water, (E) $\delta^{18}O$ of precipitation, (F) $\delta^{18}O$, and (G) δD of drip water (DW1# and MP1–MP5) in Furong Cave. (H) Monthly precipitation and average air temperature outside of Furong Cave. The red dashed arrows indicate the increase in the Mg/Ca ratio in the drought years (2006, 2009, and 2011, shaded by pink bands), and the blue dashed arrows indicate the decrease in the Mg/Ca ratio in the wet years (2007 and 2016, shaded by light blue bands). The red dashed boundary rectangles indicate the 1000*Sr/Ca increase in winter and spring in (C). The red and blue dashed boundary rectangles in (F) and (G) indicate the potential response of the drip water $\delta^{18}O/\delta D$ to ENSO, presented by the abnormal change in $\delta^{18}O/\delta D$ compared with the general smooth change in $\delta^{18}O/\delta D$ during the entire monitoring period. Detailed comparison in Appendix Fig. 4. (For interpretation of the references to colour in this figure legend, the reader is referred to the web version of this article.)

Classification of drought and wet years was based on the Dp value. A year with the Dp value being less than or equal to −15% was defined as a drought year, and that with a Dp value being above or equal to 15% was defined as a wet year (Wei et al., 2017). According to the principles of climate statistics in the China monsoon region, a year is divided into four seasons as spring (March–May), summer (June–August), autumn (September–November), and winter (December–February of the following year) (Deng et al., 2017).

ENSO frequently occurs with changes in the large-scale atmospheric circulation. The indexes of the Sea Surface Temperature Anomaly (SSTA) of the Niño 3.4 zone (5 °N–5 °S, 170 °W–120 °W) are commonly used to define ENSO (Ropelewski and Jones, 1987; Trenberth, 1997). According to the definition by the National Oceanic and Atmospheric Administration, USA, if the three-month sliding average of SSTA in the

Niño 3.4 zone is ≥0.5 °C (≤ −0.5 °C) and lasts for five consecutive months, the event can be defined as an El Niño (La Niña) event. The SSTA values of the Niño 3.4 zone were downloaded from the following official websites: http://www.cpc.ncep.noaa.gov/data/indices/sstoi.indices (SSTA).

3.2. Stable isotopic composition of rainwater

On the basis of the principles of Global Network of Isotopes in Precipitation drafted by International Atomic Energy Agency (https://nucleus.iaea.org/wiser/index.php), rainwater samples for stable isotope analyses were collected outside of Furong Cave during the period from May 2006 to September 2016. Approximately 1 cm thick liquid paraffin was filled into the rainwater-collection barrel to prevent the evaporation. In addition, foam insulation and tinfoil paper were used to cover the barrel to prevent the effect of solar radiation on the chemical composition of rainwater. The collected rainwater was regularly sampled at the end of each month and then, preserved in a refrigerator at 5 °C. Next, 5 mL water samples were taken from these samples to evaluate the stable hydrogen and oxygen isotopic compositions.

3.3. Stable isotopic compositions and trace element ratios of drip water

Drip water samples were collected during the period of October 2005 to September 2016. The sites of DW1# and MP3 were monitored from October 2005 to September 2016, and the other drip sites were monitored from October 2008 to September 2016. Polyethylene bottles and caps for sample collecting were boiled for 5 h in a 1:5 vol ratio of nitric acid, then washed with ultra-pure water, and dried out naturally in an ultra-clean room (Bench, class 100 clean). For each monitoring site, 50 mL of drip water was filtered through pre-washed 0.45-μm Millipore nitrocellulose filters, packaged in a cleaned polyethylene bottle, and acidified to pH < 2.0 by adding a trace level of ultrapure HNO_3 (1:1 volume ratio) for the analyses of trace elements. The concentrations of cations Ca^{2+}, Mg^{2+}, Ba^{2+}, and Sr^{2+} were measured with the Optima 2100DV inductively coupled plasma emission spectrometer (ICP-OES, Perkin-Elmer, USA). The detection limit was 1 μgL^{-1}, and the analytical error was ≤2%. The collection and analytical methods of the deposition rate and trace element compositions of the active deposits under the monitored drip water referred to Huang et al. (2015).

Furthermore, 5 mL of drip water for the analysis of $\delta^{18}O/\delta D$ was collected and stored in the refrigerator at 5 °C. The isotopic composition ($\delta^{18}O/\delta D$) of the rainwater and drip water samples was determined with a liquid water isotope analyzer (LWIA DLT-100, Los Gatos Research, USA). 1.5 mL volumes of water samples were analyzed 6 times, and the average of the last four measurements was used to calculate the value of the measured sample. LGR3A, LGR4A, LGR5A (Los Gatos Research, USA) were used as reference standards to be cross-checked. The analytical absolute error for $\delta^{18}O$ was ± 0.2‰ and ± 0.5‰ for δD. The result of $\delta^{18}O/\delta D$ was presented as the relative value to Vienna Standard Mean Ocean Water (V-SMOW) value (Zhou and Li, 2017):

$$\delta^{18}O = [(18O/16O)_{sample} - (18O/16O)_{V-SMOW}]/(18O/16O)_{V-SMOW} \times 10^3‰$$

$$\delta D = [(D/H)_{sample} - (D/H)_{V-SMOW}]/(D/H)_{V-SMOW} \times 10^3‰$$

3.4. Discharge of drip water and pCO_2 of soil and cave air

During the period from January 2010 to September 2016, 20-mL cylinders were used to measure the discharge of drip water (mL/min). The variation in the cave air pCO_2 concentration was monitored near the drip water sites (MP1–MP4) with a handheld Testo 535 CO_2 monitor, made in Germany. The measuring range was 0–9999 ppm for the instrument, and the resolution was higher than 1 ppm with an error of ± 2%. There were no measured pCO_2 data for DW1# and MP5, because the distance between DW1# and MP1 was merely 3 m, and the distance between MP4 and MP5 was only 1.5 m (Fig. 1C). During the period from July 2010 to September 2016, CO_2 concentration of soil air was monitored above Furong Cave (Appendix Fig. 1A). Soil air was pumped out by the collector AP-20, and the CO_2 concentration of soil air was determined by the detector tube 126SA, Komyokk, Japan, with a precision of > 100 ppm.

4. Model of PCP/ICD and WRI

According to Mg/Ca and Sr/Ca ratios of the active cave sediments and drip water, trace element distribution coefficients of Kd_{Mg} and Kd_{Sr} between H_2O and $CaCO_3$ could be calculated (Morse and Bender, 1990; Huang and Fairchild, 2001; Day and Henderson, 2013). The specific calculation formulas are as follows:

$$Kd_{Mg} = \frac{(Mg/Ca)_{crystal}}{(Mg/Ca)_{solution}} \quad (2)$$

$$Kd_{Sr} = \frac{(Sr/Ca)_{crystal}}{(Sr/Ca)_{solution}} \quad (3)$$

where Kd_{Mg} and Kd_{Sr} are the distribution coefficients of Mg and Sr, respectively.

The processes of PCP, ICD and WRI in the epikarst zone may influence the ratios of Mg/Ca and Sr/Ca in drip water (Roberts et al., 1998; Tremaine and Froelich, 2013; Casteel and Banner, 2015). Before the groundwater reached the ceiling of the cave to form drip water, carbonate was deposited in the epikarst zone along with the degassing of CO_2 (Wong et al., 2011). During the process of deposition, Ca^{2+} deposited preferentially over Mg^{2+} and Sr^{2+}, which contributed to the reduction of Ca^{2+} in the drip water and increased the Mg/Ca and Sr/Ca ratios in the drip water and the speleothem (Tremaine and Froelich, 2013). This hydrochemical process has been defined as PCP (Morse and Bender, 1990; Huang and Fairchild, 2001; Day and Henderson, 2013). ICD is another interaction between calcite and water, which takes place as the elements (Mg^{2+} and Sr^{2+}) dissolve preferentially into solution relative to Ca^{2+} (Fairchild et al., 2000; Sinclair, 2011; Sinclair et al., 2012; Casteel and Banner, 2015), particularly on the fresh surface of the calcite mineral (Brantley, 2008). It also results in an increase in Mg/Ca and Sr/Ca. For speleothems and drip water, an obvious positive correlation between Mg/Ca and Sr/Ca may be associated with PCP and ICD. Because either PCP (preferential precipitation of Ca^{2+}) or ICD (preferential dissolution of Mg^{2+} and Sr^{2+}) may increase the Mg/Ca and Sr/Ca ratios, PCP and ICD are indistinguishable in the epikarst (Sinclair et al., 2012; Casteel and Banner, 2015). In this article, these two processes are combined as PCP/ICD. In contrast, WRI generally indicates the recrystallization of calcite/dolomite or the incongruent dissolution of dolomite. Even with the effect of PCP/ICD, WRI may result in an increase in Mg/Ca and Sr/Ca ratios of the solution (Fairchild et al., 2000; Musgrove and Banner, 2004; Wong et al., 2011).

On the basis of Kd_{Mg} and Kd_{Sr}, Sinclair proposed the PCP–ICD–WRI model for Mg/Ca and Sr/Ca ratios of drip water, utilizing the value of $(Kd_{Sr} - 1)/(Kd_{Mg} - 1)$ to assess the different effects of PCP/ICD and WRI on drip water with groundwater passing through the epikarst zone (Sinclair, 2011, Sinclair et al., 2012).

Simulation results indicated that when the residence time of groundwater in the epikarst zone was relatively short ($t \to 0$), the slope of ln(Sr/Ca) versus ln(Mg/Ca) for drip water tended to be close to the value of $(Kd_{Sr} - 1)/(Kd_{Mg} - 1)$ (Fig. 5 in Sinclair, 2011), and the drip water was obviously influenced by PCP/ICD. In contrast, with an increase in the residence time of groundwater, the slope of ln(Mg/Ca) versus ln(Sr/Ca) got closer to zero, and the drip water was mainly influenced by WRI (Fig. 5 in Sinclair, 2011).

On the basis of the values of Kd_{Sr} and Kd_{Mg} presented by Banner

(1995) and Huang and Fairchild (2001), Sinclair proposed a possible range of $(Kd_{Sr} - 1)/(Kd_{Mg} - 1)$, 0.709–1.003 (Sinclair et al., 2012). The model results showed that the slopes of ln(Mg/Ca) versus ln(Sr/Ca) falling in the range of $(Kd_{Sr} - 1)/(Kd_{Mg} - 1)$ of 0.709–1.003, proving the leading role of PCP/ICD processes when the groundwater passing through the epikarst zone to form drip water (Sinclair et al., 2012; Casteel and Banner, 2015). In contrast, mixed WRI and PCP/ICD processes were indicated by slopes under 0.709. Lower slope reflected stronger WRI (Sinclair, 2011; Sinclair et al., 2012). On the basis of the above-mentioned conclusions, Casteel and Banner monitored Texas Cave, USA, and noted significant differences in the effects of PCP/ICD and WRI between the high discharge sites and the low discharge sites (Casteel and Banner, 2015). In addition, Tadros et al. found obvious differences in the effects of PCP/ICD and WRI between the drought years and the wet years in Harrie Wood Cave, Australia (Tadros et al., 2016).

5. Results

5.1. Annual rainfall and discharge of drip water

The average annual precipitation outside of Furong Cave was 1079 mm during the period of 2005–2016. The annual precipitations in year 2006, 2009, and 2011 were 850, 751, and 847 mm, respectively, which were 229, 328, and 232 mm lower than the 12-year average value, respectively. In contrast, the Dp values were −27%, −44%, and −27%, respectively, which were lower than −15%. Accordingly, the three years were classified as drought. The annual precipitations of 2007 and 2016 were 1352 and 1498 mm, respectively, which were 273 and 419 mm higher than 1079 mm, respectively. At the same time, the Dp values were 20%, and 27%, respectively, which were higher than 15%. These two years were classified as wet. The precipitations of the other years were relatively close to the 12-year average value, and thus, these years were classified as normal (Fig. 2A and H).

The average discharge monitored at the six drip water sites (DW1# and MP1–MP5) in Furong Cave were 8.7, 11.7, 20, 4.9, 1.3, and 0.7 mL/min, respectively (Appendix Table 1). With the discharge of 8 mL/min as the standard, the six drip water sites were divided into high discharge sites (DW1#, MP1, and MP2) and low discharge sites (MP3, MP4, and MP5). The standard deviation (SD) of the discharge at the high discharge sites was higher than that at the low discharge sites (Appendix Table 1), indicating that the high discharge sites responded more sensitively to the external climatic situation. Moreover, the discharge at different drip water sites varied considerably, which can be attributed to the differences in the thickness of overlying strata and the flow path of groundwater through the epikarst zone (Huang et al., 2016). At the same time, the discharge of MP2 site exhibited a relative remarkable response to external precipitation (Appendix Fig. 2D and E), which presented in high discharge corresponding to local precipitation, indicating less residence time compared with others drip sites (Huang et al., 2016).

5.2. Mg/Ca, Sr/Ca, and Ba/Ca of drip water

The Mg/Ca values for all drip water samples (DW1# and MP1–MP5) are summarized in Table 1. Although no clear seasonal characteristics were identified (Fig. 2B), the Mg/Ca values in the winter season were higher than that in the summer season (Fig. 3A). The variation ranges for 1000*Sr/Ca and for all the drip water monitoring sites (DW1# and MP1–MP5) were 0.55–1.11 (Table 1). Seasonal characteristics were observed for the changes of 1000*Sr/Ca for all drip water samples, with higher values in winter and spring and lower values in summer and autumn, except for the winter of 2010–2011 (Fig. 2C). On the other hand, the average value of drip water 1000*Sr/Ca in summer was lower than that in winter for all drip water sites (Fig. 3B), which also confirmed the seasonal changes in 1000*Sr/Ca. A similar trend was observed for the change in 1000*Ba/Ca for the drip water at all sites, but the absolute values were considerably different among these monitoring sites. For example, the average value of 1000*Ba/Ca for MP1 was approximately three times that for MP3 (Table 1 and Fig. 2D).

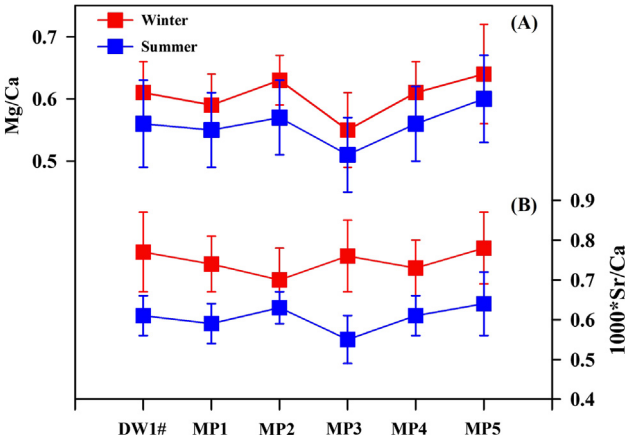

Fig. 3. (A) Mean value of Mg/Ca in the drip water for the summer and winter seasons (DW1# and MP1–MP5). (B) The mean value of 1000*Sr/Ca in the drip water for the summer and winter seasons (DW1# and MP1–MP5). The error bars represent the standard deviation (SD) of the drip water Mg/Ca and 1000*Sr/Ca values at different monitoring sites.

5.3. $\delta^{18}O$ and δD in meteoric water and drip water

The $\delta^{18}O$ of precipitation exhibited an obvious seasonal variation with lighter values in summer and heavier values in winter (Fig. 2E). Based on $\delta^{18}O$ and δD values of the rainwater samples outside Furong Cave, the equation of the local meteoric water line (LMWL) was $\delta D = 9.06\delta^{18}O + 20.44$, and the correlation coefficient was $R = 0.99$ ($p < 0.01$) (Fig. 4).

The $\delta^{18}O$ and δD values of drip water (DW1# and MP1–MP5) changed in the range from −8.9‰ to −4.3‰ and from −51.2‰ to −38.1‰, respectively (Table 1), which were distributed around the LMWL, indicating that the drip water preserved the isotopic signal of precipitation (Fig. 4).

5.4. Calculation results of PCP/ICD and WRI model

The Kd_{Mg} and Kd_{Sr} values of active sediments/drip water system in

Table 1
Medians and ranges for the Mg/Ca, 1000*Sr/Ca, 1000*Ba/Ca, and the $\delta^{18}O/\delta D$ values for drip water (DW1#, MP1–MP5) in Furong Cave.

	Mg/Ca	1000*Sr/Ca	1000*Ba/Ca	$\delta^{18}O$ (‰)	δD (‰)
DW1#	0.58 (0.39–0.79)	0.75 (0.55–1.00)	1.22 (0.81–1.70)	−7.0 (−8.8–−5.4)	−44.7 (−50.0–−38.5)
MP1	0.57 (0.39–0.78)	0.73 (0.58–0.96)	1.42 (0.95–1.98)	−7.0 (−8.9–−5.2)	−44.2 (−49.4–−39.0)
MP2	0.60 (0.41–0.71)	0.68 (0.58–0.90)	0.89 (0.65–1.41)	−7.2 (−8.9–−4.3)	−45.3 (−50.5–−38.1)
MP3	0.52 (0.34–0.73)	0.75 (0.55–1.06)	0.45 (0.20–1.12)	−7.2 (−7.8–−6.2)	−44.9 (−51.2–−40.1)
MP4	0.59 (0.40–0.78)	0.72 (0.61–0.94)	1.18 (0.44–1.49)	−7.4 (−8.0–−5.9)	−47.3 (−49.2–−42.4)
MP5	0.61 (0.42–0.90)	0.76 (0.58–1.11)	1.23 (0.33–1.93)	−7.5 (−8.0–−5.6)	−47.3 (−48.9–−41.7)

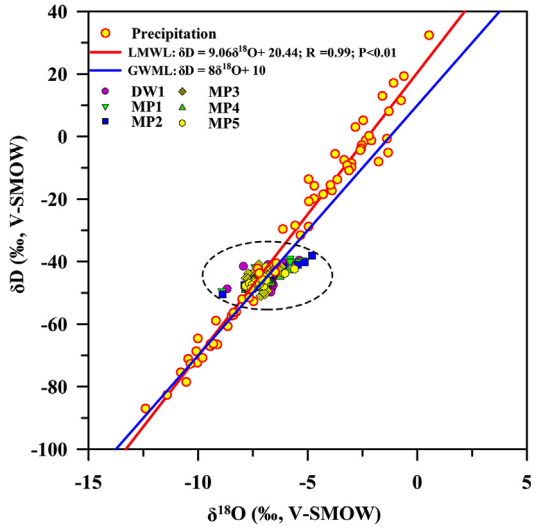

Fig. 4. Local meteoric water line (LMWL) (red line) based on the $\delta^{18}O$ and δD values (yellow dots with red edge) of precipitation outside of Furong Cave. The global meteoric water line (GMWL, blue line; Craig, 1961) is plotted for comparison. The $\delta^{18}O$ and δD values for drip waters (DW1# and MP1–MP5) in Furong Cave distributed around the LMWL with a depressed amplitude as compared to that of precipitation (Zhou and Li, 2017), because of the "mixing effect" by the 300–500-m-thick aquifer zone above Furong Cave (Li et al., 2011). (For interpretation of the references to colour in this figure legend, the reader is referred to the web version of this article.)

Furong Cave during 2009–2016 were calculated using equations (1) and (2). The ranges of Kd_{Mg} and Kd_{Sr} were 0.02–0.09 and 0.04–0.31, with the average value being 0.03 and 0.16, respectively. Thus, we calculated the value of $(Kd_{Sr} - 1)/(Kd_{Mg} - 1)$ for the drip water in Furong Cave. It fluctuated in the range of 0.727–0.988, falling within the predicted range of 0.709–1.003 from Sinclair et al. (2012) (Appendix Fig. 3). In general, for all drip water samples in Furong Cave, the slope of ln(Mg/Ca) versus ln(Sr/Ca) varied from 0.17 to 0.39 (Fig. 5A and B). The slopes of ln(Mg/Ca) versus ln(Sr/Ca) in wet year and drought year are 0.31 and 0.24, respectively, and a reduced slope of ln(Mg/Ca) versus ln(Sr/Ca) was found in drought years (Fig. 5C).

6. Discussions

6.1. Causes for the change of trace element ratios

The changes of Mg/Ca ratio in drip water responded to the changes in local hydrological conditions (drought and wet) on interannual scale (Fig. 2B). During the drought years (2006, 2009, and 2011) with decreased precipitation (Fig. 2A), more trace elements were dissolved from the bedrock because of the extended residence time of groundwater and enhanced WRI. In general, dissolution of calcite was faster than that of dolomite. With enhanced WRI, more dolomite dissolved and more Mg^{2+} released into groundwater (Fairchild et al., 2000). In addition, the occurrence of PCP with preferential deposition of Ca^{2+} relative to Mg^{2+} and Sr^{2+} also resulted in a higher Mg/Ca ratio (Karmann et al., 2007; Wong et al., 2011; Tremaine and Froelich, 2013; Casteel and Banner, 2015). In contrast, in wet years with increased precipitation (2007 and 2016, Fig. 2A), groundwater penetrated rapidly, shortening the time of WRI. What's more, accelerated bedrock dissolution resulted from higher contribution of rainwater can increase the concentration of metal ions, with more increase of Ca^{2+} compared to Mg^{2+} and finally lead to lower Mg/Ca (Fig. 2B).

In theory, the distribution coefficient of Mg between solution and calcite was mainly determined by temperature (Mucci and Morse, 1983; Morse and Bender, 1990). Therefore, the cave temperature was also considered as a potential factor for the evolution of the Mg/Ca ratio in the drip water (Gascoyne, 1983; Huang and Fairchild, 2001). However, air temperature in Furong Cave was stable at 16.0–16.3 °C (Li et al., 2011). Therefore, air temperature in Furong Cave was not a main reason for the evolution of Mg/Ca ratio in drip water. In summary, changes in precipitation and WRI were the main reasons for the evolution of Mg/Ca ratio of drip water in dry and wet years.

Correlation coefficients (R) between the concentration of Ca^{2+} and 1000*Sr/Ca, and that between the concentration of Sr^{2+} and 1000*Sr/Ca of the drip water in Furong Cave were 0.52 ($p < 0.01$) and 0.22 ($p < 0.01$) respectively (Fig. 6C and 6D), which indicated that the change of 1000*Sr/Ca was mainly controlled by the concentration of Ca^{2+}. The occurrence of PCP during the drought months of winter and spring with the deposition of Ca^{2+} accounted for the increase in 1000*Sr/Ca in drip water. The pCO_2 of cave air was also an important factor for the evolution of 1000*Sr/Ca ratio in drip water (Burton and Walter, 1991; Banner et al., 2007; Wong et al., 2011; Sherwin and Baldini, 2011; Treble et al., 2015). In summer months, the average values of soil air CO_2 concentrations at five monitoring sites (SA, SB, SC, SD, SE) above Furong Cave were 7974, 8096, 7286, 5028, 8524 ppm, respectively, and the cave air CO_2 concentrations at four monitoring sites (MP1, MP2, MP3, MP4) in Furong Cave were 1390, 1523, 1537, and 1386 ppm, respectively. In contrasts, in winter months, the average values of soil air CO_2 concentrations at the five monitoring sites were 1481, 1793, 592, 898, 662 ppm, and the cave air CO_2 concentrations at four monitoring sites (MP1, MP2, MP3, MP4) in Furong Cave were 1071, 1045, 1115, 1209 ppm, respectively. Monitoring results showed a significant seasonal variation of air pCO_2 in the soil and cave air, which was higher in summer months and lower in winter

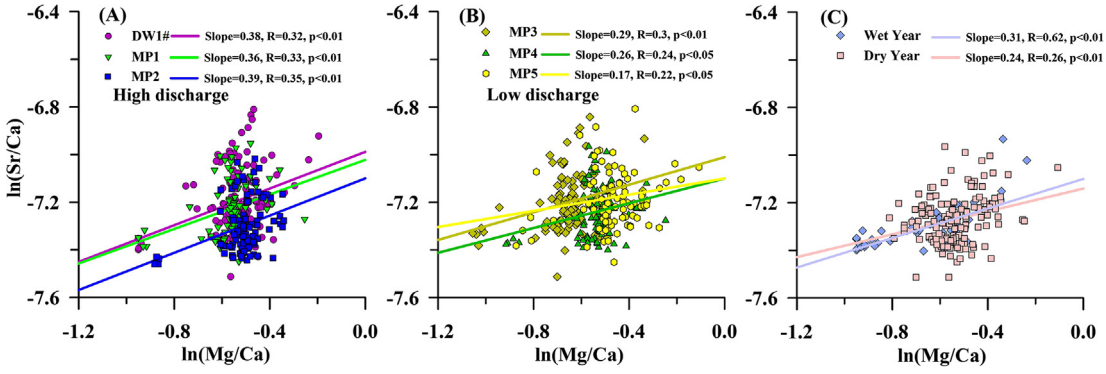

Fig. 5. Response of the hydrochemical composition of drip waters to regional rainfall (wet/drought) via the ln(Mg/Ca) *vs.* ln(Sr/Ca) curve of drip waters in Furong Cave. (A) ln(Mg/Ca) *vs.* ln(Sr/Ca) for the high discharge drip sites (DW1#, MP1, and MP2); (B) ln(Mg/Ca) *vs.* ln(Sr/Ca) for the low discharge drip sites (MP3–MP5); (C) ln(Mg/Ca) *vs.* ln(Sr/Ca) in the wet years (2007 and 2016) and drought years (2006, 2009, and 2011). Lower slope of ln(Mg/Ca) *vs.* ln(Sr/Ca) indicates a strengthened water–rock interaction (WRI) (Sinclair, 2011; Sinclair et al., 2012).

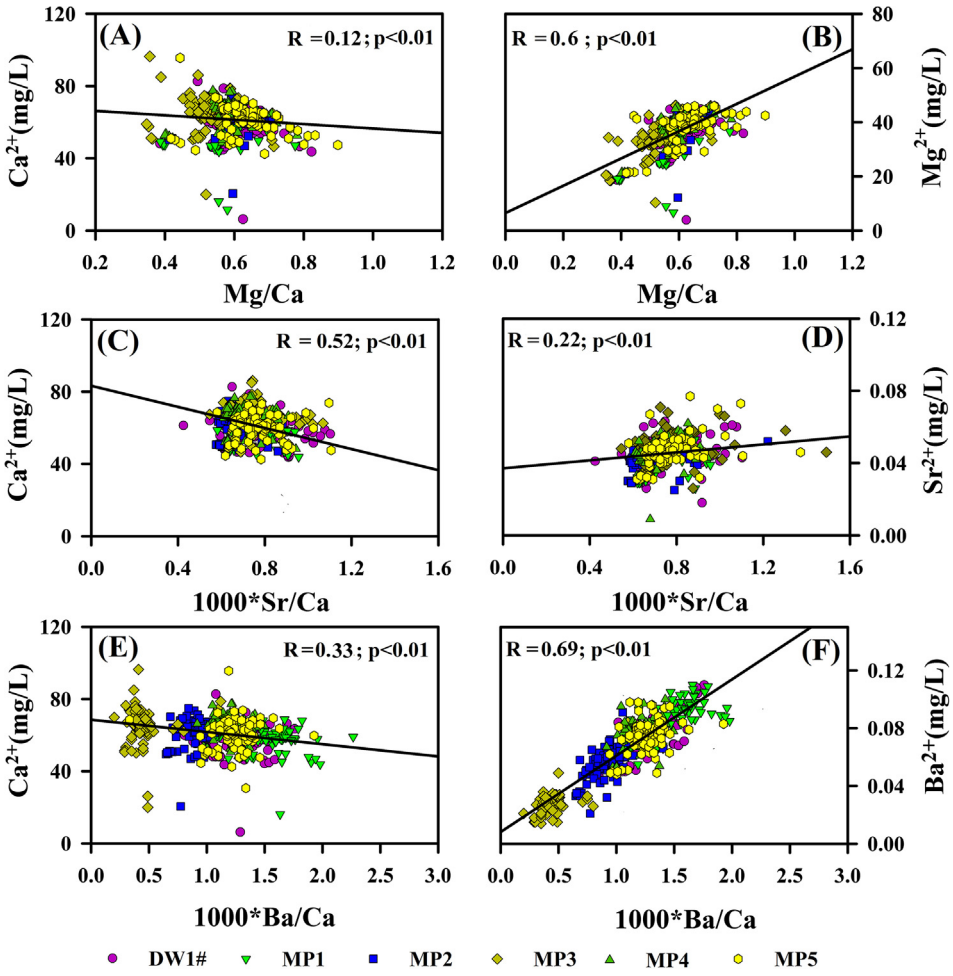

Fig. 6. Correlation among the concentrations of Ca^{2+}, Mg^{2+}, and Sr^{2+} with Mg/Ca, 1000*Sr/Ca, and 1000*Ba/Ca for the drip waters (DW1# and MP1–MP5) in Furong Cave. (A) Ca^{2+} *vs.* Mg/Ca; (B) Mg^{2+} *vs.* Mg/Ca; (C) Ca^{2+} *vs.* 1000*Sr/Ca; (D) Sr^{2+} *vs.* 1000*Sr/Ca; (E) Ca^{2+} *vs.* 1000*Ba/Ca; (F) Ba^{2+} *vs.* 1000*Ba/Ca.

months. The change in cave air pCO_2 lagged by 1–2 months compared with that in soil (Appendix Fig. 2A and B, Li and Li, 2018). In addition, an obvious correlation was observed between cave air pCO_2 and soil CO_2, except for SC–MP1 and SE–MP3 (Appendix Table 2), indicating that the change in cave air pCO_2 was mainly controlled by soil CO_2 (Li and Li, 2018). With an increase of precipitation in summer months, enhanced biological activities led to massive soil CO_2 entering the cave through groundwater and fissures, resulting in an increase in pCO_2 of cave air (Breecker et al., 2012; Meyer et al., 2014). The increase in cave air pCO_2 depressed the degassing of CO_2 from the cave water and the deposition of speleothem (Baldini et al., 2008), which also led to a lower 1000*Sr/Ca and Mg/Ca ratios in drip water (Appendix Fig. 2A, 2B, 2C; Fig. 3).

A previous study showed that 1000*Ba/Ca in soil and bedrock above Furong Cave presented a significant spatial variation and changed in the range of 4.27–59.28 and 0.04–0.25, respectively (Xiang et al., 2011). Three types of flow patterns, namely conduit flow, fissure flow and seepage flow, have been observed when the groundwater migrates through the vadose zone (Baldini et al., 2006). The migration rate was considerably different for these three types of flows, resulting in different residence time of the groundwater in the bedrock and the soil, finally leading to different dissolution rate of minerals from the soil and the bedrock (Fairchild et al., 2006), and obviously different values of 1000*Ba/Ca for all these drip sites. It is plausible that considerable effect of the soil and the bedrock overlying Furong Cave shielded the response of 1000*Ba/Ca in drip water to the change in local precipitation. The correlation coefficient (R) between the concentration of Ba^{2+} and 1000*Ba/Ca was 0.69 ($p < 0.01$), which was significantly higher than that between the concentration of Ca^{2+} and 1000*Ba/Ca ($R = 0.33$, $p < 0.01$) (Fig. 6E and F). It indicated that the change in Ba^{2+} exerted a larger influence on the change in 1000*Ba/Ca than Ca^{2+} did. Therefore, the deposition of Ca^{2+} was not the major reason for the change in 1000*Ba/Ca in drip water. No seasonal characteristics were observed for the change in 1000*Ba/Ca (Fig. 2D), which might be attributed to the different spatial distributions of Ba^{2+} concentrations in the soil and the bedrock overlying Furong Cave (Xiang et al., 2011).

6.2. Causes for the change of $\delta^{18}O$ and δD in meteoric water and drip water

Compared with the global meteoric water line (GMWL) $\delta D = 8\delta^{18}O + 10$ (Craig, 1961), there was a greater slope and intercept in the local meteoric water line (LMWL) (Fig. 4), which can be attributed to the difference in moisture sources in different seasons for this monsoon prevailing area. For this region, in rainy season (summer months), the moisture mainly comes from the tropical ocean (e.g., Indian Ocean) (Ding and Liu, 2008; Liu et al., 2008, 2010). While in dry seasons of winter and spring, the moisture mainly comes from continent air mass transported by the Westerlies, and the revaporizing vapor from local water sources. The stable isotopes of hydrogen and oxygen in the moisture and the vapor were fractionated several times in the processes of transportation and revaporization, resulting in a larger slope and intercept in the LMWL (Li et al., 2010; Zhou and Li, 2017). On the other hand, no clear seasonal change in $\delta^{18}O$ and δD of drip water was observed (Fig. 2F and G), which was attributed to the "mixing effect" of

the groundwater when it flowed through the vadose zone (Pape et al., 2010; Li et al., 2011; Partin et al., 2013; Genty et al., 2014). The thickness of overlying strata was 300–500 m above Furong Cave, which resulted in a long residence time of the precipitation and groundwater in the bedrock, smoothening the seasonal signals of $\delta^{18}O$ and δD in the precipitation (Li et al., 2011).

Although the "mixing effect" of the groundwater depressed the changes in $\delta^{18}O$ and δD in drip water, a significant change of drip water $\delta^{18}O$ and δD was observed in the winter of 2009 and the winter–spring of 2014–2015 (Fig. 2F and G). Previous reports on Mulu karst system (4°N, 114°E) in northwestern Borneo, Yangkou Cave (29°02′N, 107°11′E) in southwest China and Jiguan Cave (33°46′N, 111°34′E) in central China indicated that $\delta^{18}O$ of cave drip water did make response to ENSO (Moerman et al., 2014; Chen and Li, 2018; Sun et al., 2018).

The La Niña event occurred with constant negative SSTA in the Niño 3.4 zone during 2007–2009 with the negative isotope excursion (Appendix Fig. 4A, 4B, 4C, 4D). In this situation, with the northward and eastward migration of the weakened Western Pacific Subtropical High (WPSH) (Tan and Nan, 2010; Chen and Li, 2018), vapor from distant moisture source (India Ocean) increased obviously in the monsoon region of China, and the vapor from the Western Pacific Ocean decreased (Tan, 2014; Chen and Li, 2018). The change in moisture source finally led to depleted $\delta^{18}O$ of precipitation and drip water in the monsoon region of China in the La Niña scenario.

In contrast, continuous positive SSTA in the Niño 3.4 zone indicated the formation of the El Niño event during 2014–2015 with the positive isotope excursion (Appendix Fig. 4F, 4G, 4H, 4I). In this period, the WPSH strengthened; then, migrated southward, introducing water vapor to south China along the south margin of the WPSH (Tan and Nan, 2010). With this atmospheric circulation pattern, more vapor from the relatively close moisture source, West Pacific and South China Sea, was transported into the monsoon region of China and resulted in heavier $\delta^{18}O$ in precipitation and drip water (Nan et al., 2014; Tan, 2016). In Furong Cave, the significant change in $\delta^{18}O/\delta D$ for the high discharge drip water sites in the winter of 2009 can be attributed to a La Niña event (Appendix Fig. 4A, 4B, 4C, 4D). In contrast, the higher drip water $\delta^{18}O/\delta D$ values in the winter-spring of 2014–2015 responded to an El Niño event (Appendix Fig. 4F, 4G, 4H, 4I). The decreased precipitation in 2007–2009 increased the residence time of groundwater in the epikarst zone, and then, the drip water responded to ENSO with a longer time lag than that in 2014–2015 (Appendix Fig. 4).

More importantly, no "amount effect" between the $\delta^{18}O$ of precipitation/drip water and local precipitation was observed in 2007–2009 and 2014–2015. It was found that monthly precipitation anomaly exhibited a decreased trend in 2007–2009 outside of Furong Cave (Appendix Fig. 4E). However, the $\delta^{18}O$ of precipitation and drip water were depleted during 2007–2009 (Appendix Fig. 4B, 4C, 4D). In addition, the $\delta^{18}O$ values of precipitation and drip water exhibited heavier values with local precipitation increased during 2014–2015, which was also contrary to "amount effect" (Dansgaard, 1964; Appendix Fig. 4G, 4H, 4I, 4J).

It is plausible that at least in the monitoring period, although there was a lag of several months between the response of the drip water and the local precipitation, the $\delta^{18}O$ and δD values of local precipitation and drip water collected from the high discharge monitoring sites in Furong Cave may be influenced by the changes of moisture source, which potentially have the ability to record the changes in atmospheric circulations, such as El Niño and La Niña scenarios (Zhou and Li, 2017; Chen and Li, 2018). However, further monitoring is essential to remove the randomness and confirm this inference.

6.3. Assessment on PCP/ICD and WRI for different discharge and hydrological condition

During the migration through bedrock above the cave, the precipitation and groundwater were affected by PCP/ICD and WRI in the epikarst zone with a change in trace element ratios (Tooth and Fairchild, 2003; Baldini et al., 2006; Wong et al., 2011; Casteel and Banner, 2015; Tadros et al., 2016). The slopes of ln(Mg/Ca) versus ln (Sr/Ca) in drip water samples with high discharge (DW1#, MP1, and MP2) and those in drip water samples with low discharge (MP3, MP4, and MP5) changed in the range of 0.36–0.39 and 0.17–0.29, respectively (Fig. 5A and 5B). It indicated that WRI was stronger at the low discharge sites than that at the high discharge sites. Low discharge sites were mainly supplied by a seepage flow with a relatively slow migration of groundwater, high dissolution of bedrock, and strong WRI (Casteel and Banner, 2015).

In contrast, high discharge sites were supplied by the conduit and fissure flows with a relatively high rate and weak WRI. In addition, WRI in the drought years was stronger than that in the wet years because of the minor slope of ln(Mg/Ca) versus ln(Sr/Ca) in the drought years (Fig. 5C). It can be attributed to the fact that precipitation and groundwater has longer residence times in the bedrock in drought years. All the above analyses showed that in the drought years and at the low discharge sites, the prolongation of the residence time of groundwater in bedrock and soil strengthened the process of WRI significantly (Li et al., 2013). Changes in local hydrological conditions were related to the changes in trace element ratios of drip water.

6.4. Climatic significance: comparison of trace element ratios and stable isotopes in drip water

During the period of this study, different characteristics for the changes in Mg/Ca, 1000*Sr/Ca, 1000*Ba/Ca, $\delta^{18}O$, and δD of the drip water in Furong Cave were observed (Fig. 2). There was a seasonal variation of 1000*Sr/Ca, which increased in winter and spring, and decreased in summer and autumn (Fig. 2C). However, the Mg/Ca ratio in drip water responded to the change in local hydrological conditions, i.e., increase of precipitation led to lower Mg/Ca and decrease of precipitation resulted in higher Mg/Ca (Fig. 2B).

Note that no correlation was observed between the drip water $\delta^{18}O$ and the monthly precipitation ($p > 0.1$) (Fig. 7A), indicating that drip water $\delta^{18}O$ did not exhibit the "amount effect" and could not respond sensitively to the change in the precipitation $\delta^{18}O$ (Fig. 2E, F, 7A). Although the isotopic composition of drip water inherited the isotopic signal of precipitation (Section 6.2), the 300–500-m-thick bedrock above Furong Cave led to sufficient mixing of the groundwater in the epikarst zone and shielded the seasonal change in precipitation $\delta^{18}O$ (Li et al., 2011, 2012). On the other hand, by comparing with average $\delta^{18}O$ of the drip water and monthly precipitation anomaly outside Furong Cave over the past 12 years, the $\delta^{18}O$ of drip water still follows the change of local precipitation at interannual and longer timescales (Fig. 8A and B). However, significant correlations were observed between drip water Mg/Ca ratio and monthly precipitation for all drip water sites (for DW1#, MP1, MP2, MP4, and MP5, $p < 0.01$; for MP3, $p < 0.05$), indicating that the change in drip water Mg/Ca ratio reflected the change in local precipitation (Fig. 7B). Because of the uncertainty of residence time of groundwater for each drip site, it is difficult to estimate the exact residence time of ground water under current technical conditions. Therefore, we do not take residence time of groundwater into account when calculating the correlation between the drip water $\delta^{18}O$ and Mg/Ca ratio with the monthly precipitation amount. In summary, for all drip water samples in Furong Cave, the Mg/Ca ratios and $\delta^{18}O$ had different responses to the change in external climate. The changes in Mg/Ca ratio were dominated by the variation in local precipitation (hydrological conditions), while the changes in $\delta^{18}O$ of drip water did not make sensitive response to precipitation.

The different expressions of PCP/ICD and WRI in drip water with high and low discharge in Furong Cave indicated that the speleothem fed by different drip water underwent different chemical processes. Therefore, a replication test (i.e., demonstration of similar isotopic profiles of two or more sets of speleothems; Dorale and Liu, 2009) was

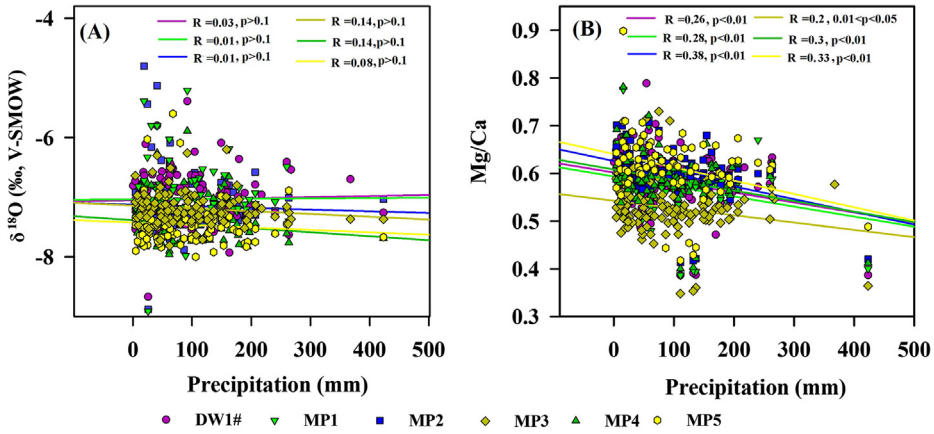

Fig. 7. (A) Correlation between $\delta^{18}O$ and monthly precipitation of drip water (DW1# and MP1–MP5). (B) Correlation between Mg/Ca and monthly precipitation of drip water (DW1# and MP1–MP5).

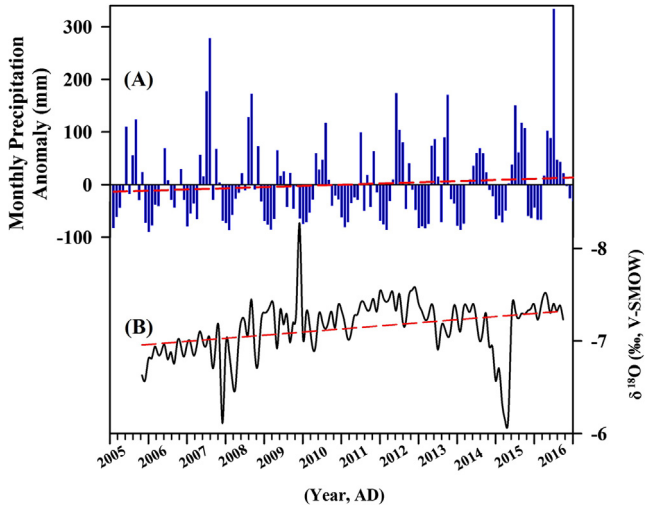

Fig. 8. (A) Monthly precipitation anomaly (mm) in the 12-year monitoring period from 2005 to 2016. (B) Monthly average $\delta^{18}O$ of the drip water for six drip sites. The fitting dashed red lines indicated the trend for the changes in monthly precipitation anomaly and $\delta^{18}O$ of the drip water. Monthly precipitation anomaly is equal to the monthly precipitation minus the average multi-month precipitation. (For interpretation of the references to colour in this figure legend, the reader is referred to the web version of this article.)

more scientifically reliable and robust in paleoclimate reconstruction based on the records of speleothem.

Series of abrupt climatic events on the centennial-millennial time scales, such as Greenland Interstadials, Heinrich events, and Younger Dryas, have been recorded by the speleothem records from the China monsoon regions (Wang et al., 2001, 2008; Li et al., 2007, 2014, 2017; Han et al., 2016; Zhang et al., 2017). The speleothem $\delta^{18}O$ in Furong Cave also recorded the change in ASM at the termination of the Last Glacial period (Li et al., 2011). No correlation was observed between the $\delta^{18}O$ of drip water and local rainfall assuming no time lag between drip water and local meteoric water (Fig. 7A). In contrast, change in trace element ratios of drip water eventually made response to the change of local precipitation, indicating that the $\delta^{18}O$ and the trace element ratios reflected different climatic signals on the monthly and seasonal timescales (Figs. 2 and 7).

7. Conclusions

Based on the 12-year monitoring of the $\delta^{18}O$, δD, and trace element ratios of drip water and local hydrological conditions outside of Furong Cave, Southwest China, the main conclusions were as follows:

(1) The Mg/Ca of drip water responded to local hydrological conditions with lower values in wet years and higher values in drought years. A seasonal characteristic was observed for the change in 1000*Sr/Ca with an increase in winter and spring, and a reduction in summer and autumn. The change in Ca^{2+} with PCP had an important influence on the change in 1000*Sr/Ca of drip water.
(2) Analysis with the PCP–ICD–WRI model may reveal that the influence of WRI in the epikarst zone was stronger than that of PCP/ICD in drought years, and the influence of WRI on drip water with high discharge was weaker than that on drip water low discharge.
(3) The $\delta^{18}O$ and δD of drip water in Furong Cave preserved the isotopic signal of precipitation, and the range of seasonal change was depressed by the "mixing effect" with "old water" in the epikarst zone, without any expression of the "amount effect" on monthly timescale.
(4) The high-resolution (e.g., seasonal and annual) $\delta^{18}O$ record of speleothem in Furong Cave may not be useful. However, $\delta^{18}O$ record of speleothem in Furong Cave may follow with local precipitation on decadal and longer timescales. In addition, the trace element ratios are potentially reliable proxies in speleothems to record the change of rainfall on annual and seasonal timescales.

Declarations of interest

All authors declare no competing interests.

Acknowledgments

We would like to express our sincere gratitude to the Management Department of Furong Cave for considerable help in the field since 2005. The editor Peter K Kitanidis, associate editor Dongmei Han, and three anonymous reviewers are greatly appreciated for their constructive comments to improve the quality of this paper. This research was supported by National Natural Science Foundation of China (NSFC) (No. 41772170), and the Fundamental Research Funds for the Central Universities (Nos. XDJK2017A010 and XDJK2013A012) to T.-Y. Li. A professional English translator, Dr. Xiang Xinyi, Southwest University, China, is also greatly appreciated for her effort in polishing the final version of the manuscript.

Appendix A. Supplementary data

Supplementary data to this article can be found online at https://doi.org/10.1016/j.jhydrol.2019.02.052.

References

Baldini, J.U.L., Mcdermott, F., Fairchild, I.J., 2006. Spatial variability in cave drip water hydrochemistry: implications for stalagmite paleoclimate records. Chem. Geol. 235 (3), 390–404.

Baldini, J.U.L., Mcdermott, F., Hoffmann, D.L., Richards, D.A., Clipson, N., 2008. Very high-frequency and seasonal cave atmosphere pCO_2 variability: implications for stalagmite growth and oxygen isotope-based paleoclimate records. Earth Planet. Sci. Lett. 272 (1), 118–129.

Banner, J.L., 1995. Application of the trace element and isotope geochemistry of strontium to studies of carbonate diagenesis. Sedimentology 42 (5), 805–824.

Banner, J.L., Guilfoyle, A., James, E.W., Stern, L.A., Musgrove, M., 2007. Seasonal variations in modern speleothem calcite growth in Central Texas, U.S.A. J. Sediment. Res. 77 (7–8), 615–622.

Brantley, S.L., 2008. Kinetics of mineral dissolution. In: Brantley, S.L., Kubicki, J.D., White, A.F. (Eds.), Kinetics of Water-Rock Interaction. Springer, New York, pp. 151–196.

Breecker, D.O., Payne, A.E., Quade, J., Banner, J.L., Ball, C.E., Meyer, K.W., Cowan, B.D., 2012. The sources and sinks of CO_2 in caves under mixed woodland and grassland vegetation. Geochim. Cosmochim. Acta 96 (11), 230–246.

Burton, E.A., Walter, L.M., 1991. The effects of pCO_2 and temperature on magnesium incorporation in calcite in seawater and $MgCl_2$-$CaCl_2$ solutions. Geochim. Cosmochim. Acta 55 (3), 777–785.

Cai, B.G., Zhu, J., Ban, F.M., Tan, M., 2010. Intra-annual variation of the calcite deposition rate of drip water in Shihua Cave, Beijing, China and its implications for palaeoclimatic reconstructions. Boreas 40, 525–535.

Casteel, R.C., Banner, J.L., 2015. Temperature-driven seasonal calcite growth and drip water trace element variations in a well-ventilated Texas cave: implications for speleothem paleoclimate studies. Chem. Geol. 392, 43–58.

Chen, C.-J., Li, T.-Y., 2018. Geochemical characteristics of cave drip water respond to ENSO based on a 6-year monitoring work in Yangkou cave, Southwest China. J. Hydrol. https://doi.org/10.1016/j.jhydrol.2018.04.061.

Cheng, H., Edwards, R.L., Broecker, W.S., Denton, G.H., Kong, X.G., Wang, Y.J., Zhang, R., Wang, X.F., 2009. Ice age terminations. Science 326, 248–252.

Cheng, H., Sinha, A., Wang, X.F., Cruz, F.W., Edwards, R.L., 2012. The global paleomonsoon as seen through speleothem records from Asia and the Americas. Clim. Dyn. 39 (5), 1045–1062.

Cheng, H., Edwards, R.L., Sinha, A., Spötl, C., Yi, L., Chen, S.T., Kelly, M., Kathayat, G., Wang, X.F., Li, X.L., Kong, X.G., Wang, Y.J., Ning, Y.F., Zhang, H.W., 2016. The Asian monsoon over the past 640,000 years and ice age terminations. Nature 534 (7609), 640–646.

Clemens, S.C., Prell, W.L., Sun, Y., 2010. Orbital-scale timing and mechanisms driving late Pleistocene Indo-Asian summer monsoons: reinterpreting cave speleothem $\delta^{18}O$. Paleoceanography 25 (PA4207), 545–558.

Craig, H., 1961. Isotopic variations in meteoric waters. Science 133, 1702.

Day, C.C., Henderson, G.M., 2013. Controls on trace-element partitioning in cave-analogue calcite. Geochim. Cosmochim. Acta 120, 612–627.

Dansgaard, W., 1964. Stable isotopes in precipitation. Tellus 16 (4), 436–468.

Deng, Q., Chan, L., Wei, J., Zhao, J.P., Deng, L.J., Xiang, Y.G., 2017. Association of outdoor air pollution and indoor renovation with early childhood ear infection in China. Chemosphere 169, 288–296.

Ding, Y.H., Liu, Y.Y., 2008. A study of the teleconnections in the Asian-Pacific monsoon region. Acta Meteorol. Sin. 22 (4), 404–418.

Dorale, J.A., Liu, Z.H., 2009. Limitations of Hendy test criteria in judging the paleoclimatic suitability of speleothems and the need for replication. J. Cave Karst Stud. 71 (1), 73–80.

Duan, W.H., Cai, B.G., Tan, M., Liu, H., Zhang, Y., 2012. The growth mechanism of the aragonitic stalagmite laminae from Yunnan Xianren Cave, SW China revealed by cave monitoring. Boreas 41, 113–123.

Duan, W.H., Ruan, J.Y., Luo, W.J., Li, T.Y., Tian, L.J., Zeng, G.N., Zhang, D.Z., Bai, Y.J., Li, J.L., Tao, T., Zhang, P.Z., Baker, A., Tan, M., 2016. The transfer of seasonal isotopic variability between precipitation and drip water at eight caves in the monsoon regions of China. Geochim. Cosmochim. Acta 183, 250–266.

Fairchild, I.J., Borsato, A., Tooth, A.F., Frisia, S., Hawkesworth, C.J., Huang, Y.M., McDermott, F., Spiro, B., 2000. Controls on trace element (Sr-Mg) compositions of carbonate cave waters: implications for speleothem climatic records. Chem. Geol. 166 (3–4), 255–269.

Fairchild, I.J., Smith, C.L., Baker, A., Fuller, L., Spötl, C., Mattey, D., McDermott, F., 2006. Modification and preservation of environmental signals in speleothems. Earth-Sci. Rev. 75 (1), 105–153.

Fairchild, I.J., Treble, P.C., 2009. Trace elements in speleothems as recorders of environmental change. Quat. Sci. Rev. 28 (5), 449–468.

Gascoyne, M., 1983. Trace-element partition coefficients in the calcite-water system and their paleoclimatic significance in cave studies. J. Hydrol. 61 (1–3), 213–222.

Genty, D., Labuhn, I., Hoffmann, G., Danis, P.A., Mestre, O., Bourges, F., Wainer, K., Massault, M., Van Exter, S., Régnier, E., Orengo, Ph., Falourd, S., Minster, B., 2014. Rainfall and cave water isotopic relationships in two South-France sites. Geochim. Cosmochim. Acta 131 (5), 323–343.

Han, L.-Y., Li, T.-Y., Cheng, H., Edwards, R.L., Shen, C.-C., Li, H.-C., Huang, C.-X., Li, J.-Y., Yuan, N., Wang, H.-B., Zhang, T.-T., Zhao, X., 2016. Potential influence of temperature changes in the Southern Hemisphere on the evolution of the Asian summer monsoon during the last glacial period. Quat. Int. 392, 239–250.

Huang, C.-X., Li, T.-Y., Han, L.-Y., Li, J.-Y., Yuan, N., Wang, H.-B., Zhang, T.-T., Zhao, X., 2015. Deposition rates and element features of active sediments under drip water in Furong Cave of Chongqing. Carsol. Sin. 34 (3), 238–246 (In Chinese with English abstract and figures).

Huang, C.-X., Li, T.-Y., Han, L.-Y., Li, J.-Y., Yuan, N., Wang, H.-B., Zhang, T.-T., Zhao, X., Zhou, J.-L., 2016. Variation of cave water DIC-$\delta^{13}C$ and its influencing factors in Furong Cave, Chongqing. Carsol. Sin. 35 (3), 299–306 (In Chinese with English abstract and figures).

Huang, Y., Fairchild, I.J., 2001. Partitioning of Sr^{2+} and Mg^{2+} into calcite under karst-analogue experimental conditions. Geochim. Cosmochim. Acta 65 (1), 47–62.

Jo, K.N., Woo, K.S., Hong, G.H., Kim, S.H., Suk, B.C., 2010. Rainfall and hydrological controls on speleothem geochemistry during climatic events (droughts and typhoons): an example from Seopdong Cave, Republic of Korea. Earth Planet. Sci. Lett. 295 (3), 441–450.

Johnson, K.R., Hu, C.Y., Belshaw, N.S., Henderson, G.M., 2006. Seasonal trace-element and stable-isotope variations in a Chinese speleothem: the potential for high-resolution paleomonsoon reconstruction. Earth Planet. Sci. Lett. 244 (1–2), 394–407.

Karmann, I., Cruz, F.W., Oduvaldo, V.J., Burns, S.J., 2007. Climate influence on geochemistry parameters of waters from Santana-Pérolas cave system, Brazil. Chem. Geol. 244 (1), 232–247.

Lauritzen, S.E., Lundberg, J., 1999. Speleothems and climate: a special issue of the Holocene. Holocene 96 (6), 643–647.

Li, J.-Y., Li, T.-Y., Wang, J.-L., Xiang, X.-J., Chen, Y.-X., Li, X., 2013. Characteristics and environmental significance of Ca, Mg, and Sr in the soil infiltrating water overlying the Furong Cave, Chongqing, China. Sci. China Earth Sci. 56 (12), 2126–2134.

Li, J.-Y., Li, T.-Y., 2018. Seasonal and annual changes in soil/cave air pCO_2 and the $\delta^{13}C_{DIC}$ of cave drip water in response to changes in temperature and rainfall. Appl. Geochem. https://doi.org/10.1016/j.apgeochem.2018.04.002.

Li, T.-Y., Yuan, D.-X., Li, H.-C., Yang, Y., Wang, J.-L., Wang, X.-Y., Li, J.-Y., Qin, J.-M., Zhang, M.-L., Lin, Y.-S., 2007. High-resolution climate variability of southwest China during 57–70 ka reflected in a stalagmite $\delta^{18}O$ record from Xinya Cave. Sci. China Earth Sci. 50 (8), 1202–1208.

Li, T.-Y., Li, H.-C., Shen, C.-C., Yang, C.-X., Li, J.-Y., Yi, C.-C., Yuan, D.-X., Wang, J.-L., Xie, S.-Y., 2010. Study on the δD and $\delta^{18}O$ characteristics of meteoric precipitation during 2006–2008 in Chongqing China. Adv. Water Sci. 21 (6), 57–764 (In Chinese with English abstract).

Li, T.-Y., Shen, C.-C., Li, H.-C., Li, J.-Y., Chiang, H.-W., Song, S.-R., Yuan, D.-X., Lin, C.D.J., Gao, P., Zhou, L.-P., Wang, J.-L., Ye, M.-Y., Tang, L.-L., Xie, S.-Y., 2011. Oxygen and carbon isotopic systematics of aragonite speleothems and water in Furong Cave, Chongqing, China. Geochim. Cosmochim. Acta 75 (15), 4140–4156.

Li, T.-Y., Li, H.-C., Xiang, X.-J., Kuo, T.-S., Li, J.-Y., Zhou, F.-L., Chen, H.-L., Peng, L.-L., 2012. Transportation characteristics of $\delta^{13}C$ in the plants-soil-bedrock-cave system in Chongqing karst area. Sci. China Earth Sci. 55 (4), 685–694.

Li, T.-Y., Shen, C.-C., Huang, L.-J., Jiang, X.-Y., Yang, X.-L., Mii, H.-S., Lee, S.-Y., Lo, L., 2014. Stalagmite-inferred variability of the Asian summer monsoon during the penultimate glacial-interglacial period. Clim. Past. 10 (3), 1211–1219.

Li, T.-Y., Han, L.-Y., Cheng, H., Edwards, R.L., Shen, C.-C., Li, H.-C., Li, J.-Y., Huang, C.-X., Zhang, T.-T., Zhao, X., 2017. Evolution of the Asian summer monsoon during Dansgaard/Oeschger events 13–17 recorded in a stalagmite constrained by high-precision chronology from southwest China. Quat. Res. 88 (1), 121–128.

Liu, J.B., Chen, J.H., Zhang, X.J., Li, Y., Rao, Z.G., Chen, F.H., 2015. Holocene East Asian summer monsoon records in northern China and their inconsistency with Chinese stalagmite $\delta^{18}O$ records. Earth-Sci. Rev. 148, 194–208.

Liu, J.B., Chen, S.Q., Chen, J.H., Zhang, P.Z., Chen, F.H., 2017. Chinese cave $\delta^{18}O$ records do not represent northern East Asian summer monsoon rainfall. Proc. Natl. Acad. Sci. U.S.A. 114 (15), E2987.

Liu, J.R., Song, X.F., Yuan, G.F., Sun, X.M., Liu, X., Wang, Z.M., Wang, S.Q., 2008. Stable isotopes of summer monsoonal precipitation in southern China and the moisture sources evidence from $\delta^{18}O$ signature. J. Geogr. Sci. 18, 155–165.

Liu, J.R., Song, X.F., Yuan, G.F., Sun, X.M., Xin, L., Wang, S.Q., 2010. Characteristics of $\delta^{18}O$ in precipitation over eastern monsoon China and the water vapor sources. Chin. Sci. Bull. 55 (2), 200–211.

Luo, W.J., Wang, S.J., 2008. Transmission of oxygen isotope signals of precipitation-soil water-drip water and its implications in Liangfeng Cave of Guizhou, China. Chin. Sci. Bull. 53, 3364–3370.

McDermott, F., Frisia, S., Huang, Y., Longinelli, A., Spiro, B., Heaton, T.H.E., Hawkesworth, C.J., Borsato, A., Keppens, E., Fairchild, I.J., van der Borg, K., Verheyden, S., Selmo, E., 1999. Holocene climate variability in Europe: evidence from $\delta^{18}O$ and textural variations in speleothems. Quat. Sci. Rev. 18 (8), 1021–1038.

Meyer, K.W., Feng, W.M., Breecker, D.O., Banner, J.L., Guilfoyle, A., 2014. Interpretation of speleothem calcite $\delta^{13}C$ variations: evidence from monitoring soil CO_2, drip water, and modern speleothem calcite in central Texas. Geochimica. Cosmochim. Acta 142 (2), 281–298.

Moerman, J.W., Cobb, K.M., Partin, J.W., Meckler, A.N., Carolin, S.A., Adkins, J.F., Lejau, S., Malang, J., Clark, B., Tuen, A.A., 2014. Transformation of ENSO-related rainwater to drip water $\delta^{18}O$ variability by vadose water mixing. Geophys. Res. Lett. 41 (22), 7907–7915.

Morse, J.W., Bender, M.L., 1990. Partition coefficients in calcite: examination of factors influencing the validity of experimental results and their application to natural systems. Chem. Geol. 82 (90), 265–277.

Mucci, A., Morse, J.W., 1983. The incorporation of Mg^{2+} and Sr^{2+} into calcite overgrowths: influences of growth rate and solution composition. Geochim. Cosmochim. Acta 47 (2), 217–233.

Musgrove, M.L., Banner, J.L., 2004. Controls on the spatial and temporal variability of vadose dripwater geochemistry: Edwards aquifer, Central Texas. Geochim. Cosmochim. Acta 68 (5), 1007–1020.

Nan, S., Tan, M., Zhao, P., 2014. Evaluation of the ability of the Chinese stalagmite $\delta^{18}O$ to record the variation in atmospheric circulation during the second half of the 20th century. Clim. Past 10 (3), 975–985.

Oster, J., Montanēz, I., Kelley, P., 2012. Response of a modern cave system to large seasonal precipitation variability. Geochim. Cosmochim. Acta 91 (5), 92–108.
Pape, J.R., Banner, J.L., Mack, L.E., Musgrove, M., Guilfoyle, A., 2010. Controls on oxygen isotope variability in precipitation and cave drip waters, central Texas, USA. J. Hydrol. 385 (1–4), 203–215.
Partin, J.W., Cobb, K.M., Adkins, J.F., Tuen, A.A., Clark, B., 2013. Trace metal and carbon isotopic variations in cave dripwater and stalagmite geochemistry from northern Borneo. Geochem. Geophys. Geosyst. 14 (9), 3567–3585.
Roberts, M.S., Smart, P.L., Baker, A., 1998. Annual trace element variations in a Holocene speleothem. Earth Planet. Sci. Lett. 154 (1–4), 237–246.
Ropelewski, C.F., Jones, P.D., 1987. An extension of the Tahiti-Darwin southern oscillation index. Mon. Weather Rev. 115 (9), 2161–2165.
Sherwin, C.M., Baldini, J.U.L., 2011. Cave air and hydrological controls on prior calcite precipitation and stalagmite growth rates: implications for paleoclimate reconstructions using speleothems. Geochim. Cosmochim. Acta 75 (14), 3915–3929.
Sinclair, D.J., 2011. Two mathematical models of Mg and Sr partitioning into solution during incongruent calcite dissolution: Implications for dripwater and speleothem studies. Chem. Geol. 283 (3–4), 119–133.
Sinclair, D.J., Banner, J.L., Taylor, F.W., Partin, J., Jenson, J., Mylroie, J., 2012. Magnesium and strontium systematics in tropical speleothems from the western pacific. Chem. Geol. 294–295 (3), 1–17.
Spötl, C., Fairchild, I.J., Tooth, A.F., 2005. Cave air control on dripwater geochemistry, Obir Caves (Austria): implications for speleothem deposition in dynamically ventilated caves. Geochim. Cosmochim. Acta 69 (10), 2451–2468.
Sun, Z., Yang, Y., Zhao, J.Y., Tian, N., Feng, X.X., 2018. Potential ENSO effects on the oxygen isotope composition of modern speleothems: Observations from Jiguan Cave, central China. J. Hydrol. https://doi.org/10.1016/j.jhydrol.2018.09.015.
Tadros, C.V., Treble, P.C., Baker, A., Fairchild, I., Hankin, S., Roach, R., Markowska, M., McDonald, J., 2016. ENSO-cave drip water hydrochemical relationship: a 7-year dataset from south-eastern Australia. Hydrol. Earth Syst. Sci. 20, 4625–4640.
Tan, M., Nan, S.L., 2010. Primary investigation on interannual changes in the circulation effect of precipitation oxygen isotopes in monsoon China. Quat. Sci. 30 (3), 620–622 (In Chinese with English abstract and figures).
Tan, M., 2014. Circulation effect: response of precipitation $\delta^{18}O$ to the ENSO cycle in monsoon regions of China. Clim. Dyn. 42 (3–4), 1067–1077.
Tan, M., 2016. Circulation background of climate patterns in the past millennium: Uncertainty analysis and re-reconstruction of ENSO-like state. Sci. China Earth Sci. 59 (6), 1225–1241.
Tooth, A.F., Fairchild, I.J., 2003. Soil and karst aquifer hydrological controls on the geochemical evolution of speleothem-forming drip waters, Crag Cave, Southwest Ireland. J. Hydrol. 273 (1–4), 51–68.
Treble, P.C., Fairchild, I.J., Griffiths, A., Baker, A., Meredith, K.T., Wood, A., 2015. Impacts of cave air ventilation and in-cave prior calcite precipitation on Golgotha Cave dripwater chemistry, Southwest Australia. Quat. Sci. Rev. 127, 61–72.
Tremaine, D.M., Froelich, P.N., 2013. Speleothem trace element signatures: a hydrologic geochemical study of modern cave dripwaters and farmed calcite. Geochim. Cosmochim. Acta 121 (6), 522–545.
Trenberth, K.E., 1997. The definition of El Niño. Bull. Am. Meteorol. Soc. 78 (12), 2771–2777.
Wang, Y.J., Cheng, H., Edwards, R.L., An, Z.S., Wu, J.Y., Shen, C.C., Dorale, J.A., 2001. A high resolution absolute-dated Late Pleistocene monsoon record from Hulu Cave, China. Science 294, 2345–2348.
Wang, Y.J., Cheng, H., Edwards, R.L., Kong, X.G., Shao, X.H., Chen, S.T., Wu, J.Y., Jiang, X.Y., Wang, X.F., An, Z.S., 2008. Millennial-and orbital-scale changes in the East Asian monsoon over the past 224,000 years. Nature 451, 1090–1093.
Wei, K., Wang, Q.J., Zhou, B.B., He, B., 2017. Analysis of drought characteristic in Shaanxi province based on precipitation anomaly percentage. J. Soil Water Conserv. 31 (1), 318–322 (In Chinese with English abstract and figures).
Wong, C.I., Banner, J.L., Musgrove, M.L., 2011. Seasonal drip water Mg/Ca and Sr/Ca variations driven by cave ventilation: implications for and modeling of speleothem paleoclimate records. Geochim. Cosmochim. Acta 75 (12), 3514–3529.
Wong, C.I., Breecker, D.O., 2015. Advancements in the use of speleothems as climate archives. Quat. Sci. Rev. 127, 1–18.
Xiang, X.-J., Li, T.-Y., Wang, J.-L., Li, J.-Y., Chen, J.-X., Zhou, F.-L., Zhang, W.-T., Bai, Y., 2011. Geochemical characteristics of the overlying bedrock and soil, and its impact on hydro-chemistry of the drip waters in the Furong Cave, Chongqing. Carsol. Sin. 30, 193–199 (In Chinese with English abstract and figures).
Yang, H., Johnson, K.R., Griffiths, M.L., Yoshimura, K., 2016. Interannual controls on oxygen isotope variability in Asian monsoon precipitation and implications for paleoclimate reconstructions. J. Geophys. Res. Atmos. 121 (14), 8410–8428.
Yuan, D.X., Cheng, H., Edwards, R.L., Dykoski, C.A., Kelly, M.J., Zhang, M.L., Qing, J.M., Lin, Y.S., Wang, Y.J., Wu, J.Y., Dorale, J.A., An, Z.S., Cai, Y.J., 2004. Timing, duration, and transitions of the last interglacial Asian monsoon. Science 304 (5670), 575.
Zhang, T.-T., Li, T.-Y., Cheng, H., Edwards, R.L., Shen, C.-C., Spötl, C., Li, H.-C., Han, L.-Y., Li, J.-Y., Huang, C.-X., Zhao, X., 2017. Stalagmite-inferred centennial variability of the Asian summer monsoon in southwest China between 58 and 79ka B.P. Quat. Sci. Rev. 160, 1–12.
Zhou, H.Y., Feng, Y.X., Zhao, J.X., Shen, C.C., You, C.F., Lin, Y., 2009. Deglacial variations of Sr and $^{87}Sr/^{86}Sr$ ratio recorded by a stalagmite from Central China and their association with past climate and environment. Chem. Geol. 268 (3), 233–247.
Zhou, H.Y., Greig, A., Tang, J., You, C.F., Yuan, D.X., Tong, X.N., 2012. Rare earth element patterns in a Chinese stalagmite controlled by sources and scavenging from karst groundwater. Geochim. Cosmochim. Acta 83 (1), 1–18.
Zhou, J.-L., Li, T.-Y., 2017. A tentative study of the relationship between annual $\delta^{18}O\&\delta D$ variations of precipitation and atmospheric circulations-a case from Southwest China. Quat. Int. https://doi.org/10.1016/j.quaint.2017.05.038.
Zhu, X.W., Chen, W.H., Lynch, E., 2007. Wulong karst systems and as an indicator of local tectonic uplift. Carsol. Sin. 26 (2), 119–125 (In Chinese with English abstract and figures).